Determination of specific and non-specific protein–protein interactions for beta-lactoglobulin by analytical ultracentrifugation and membrane osmometry experiments†

M. J. Uttinger,‡[a] C. S. Hundschell,‡[b] V. Lautenbach,[a] S. Pusara,[c] S. Bäther,[b] T. R. Heyn,[d] J. K. Keppler,[e] W. Wenzel,[c] J. Walter,[a] M. Kozlowska,[c] A. M. Wagemans[b] and W. Peukert*[a]

Protein–protein interactions are essential for the understanding of biological processes. Specific protein aggregation is an important aspect for many biological systems. In particular, electrostatic interactions play the key role for protein–protein interactions, as many amino acids have pH-dependent charge states. Moreover, protein dissociation is directly related to the solution pH, ionic strength, temperature and protein concentration. The subtle interplay between different specific and non-specific interactions is demonstrated for beta-lactoglobulin (BLG) with a focus on low salt concentrations, thus mimicking technically relevant processing conditions. BLG is a well-characterized model system, proven to attain its monomer–dimer equilibrium strongly dependent upon the pH of the solution. In this manuscript, we present a unique combination of analytical ultracentrifugation and membrane osmometry experiments, which quantifies specific and non-specific interactions, *i.e.* in terms of the dimer dissociation constants and the second osmotic virial coefficient, at pH 3 and 7 and sodium chloride concentrations of 10 mM and 100 mM. This provides direct insight to protein–protein interactions for a system with a concentration-dependent monomer–dimer equilibrium. Moreover, using a coarse-grained extended DLVO model in combination with molecular dynamics simulations, we quantify non-specific monomer–monomer, monomer–dimer and dimer–dimer interactions as well as the binding free energy of BLG dimerization from theoretical calculations. The experimentally determined interactions are shown to be mainly governed by electrostatic interactions and further agree with free energy calculations. Our experimental protocol aims to determine non-specific and specific interactions for a dynamically interacting system and provides an understanding of protein–protein interactions for BLG at low salt concentrations.

[a] *Institute of Particle Technology, Interdisciplinary Center for Functional Particle Systems, Friedrich-Alexander-Universität Erlangen-Nürnberg, Haberstraße 9a, 91058 Erlangen, Germany. E-mail: wolfgang.peukert@fau.de*

[b] *Institute of Food Technology and Food Chemistry, Department of Food Colloids, Technical University Berlin, Straße des 17. Juni 135, 10623 Berlin, Germany*

[c] *Institute of Nanotechnology, Karlsruhe Institute of Technology, Hermann-von-Helmholtz-Platz 1, 76344 Eggenstein-Leopoldshafen, Germany*

[d] *Institute of Human Nutrition and Food Science, Division of Food Technology, Kiel University, 24118 Kiel, Germany*

[e] *Laboratory of Food Process Engineering, Wageningen University, Wageningen, The Netherlands*

† Electronic supplementary information (ESI) available: Lennard-Jones potential, xDLVO-CG calculations, determination of extinction coefficient, coarse-grained molecular B_{22} calculations, determination of dimer dissociation by means of analytical ultracentrifugation experiments, reduced osmotic pressure from membrane osmometry measurements, monomer–dimer equilibrium: fraction of monomer and dimer, umbrella sampling simulations: potential of mean force. See DOI: https://doi.org/10.1039/d2sm00908k

‡ These authors contributed equally to the manuscript.

Introduction

Understanding the nature of protein–protein interactions (PPIs) is essential to explain biological systems and their function in biological processes. PPIs determine the properties of proteins, such as protein aggregation,[1] assembly, gel formation or stabilization,[2–4] thus influencing their subsequent biological function and commercial use. Moreover, an essential aspect of the systems behavior is the statistical mechanics of the system, which can be described through the chemical potential of the system.[5,6] Both, specific and non-specific interactions are the driving force for the particular behavior of macromolecules. On the one hand, specific interactions refer to a directed oligomerization, *i.e.* the formation of a new species.[7–10] On the other hand, non-specific interactions refer to van der Waals forces (vdW) and electrostatic interactions,

where the latter originate from dipole–dipole and charge–charge interactions. In particular, non-specific interactions significantly affect transport properties such as sedimentation and diffusion of proteins and its oligomers at finite particle concentrations, which can be taken into account by respective interaction parameters, *i.e.* the Gralen coefficient and the second virial coefficient.[11] In this context, electrostatic interactions are a central aspect of PPIs, as many amino acids have pH-dependent charge states.[12] In aqueous solution, especially upon changes of the ionic strength, controlled protein aggregation and oligomerization is significantly pronounced in the proximity of the isoelectric point, hence for a protein net charge of zero. Yet, protein aggregation and oligomerization also occurs at pH values dissimilar to the isoelectric point for changed solvent conditions or in different solvents such as ethanol.[13] In this manuscript, we target the experimental determination of both, association (specific PPIs) and concentration non-ideality (non-specific PPIs) for dynamically interacting systems, which remains a great challenge and requires careful experimental protocols.[14] The understanding of such systems is especially relevant with respect to applications in food technology, where controlled protein oligomerization can be induced by mechanical stress and can be controlled or prevented by adjusting the salt concentration.[15 18] In particular, protein aggregation is a relevant mechanism in food applications.[19] Moreover, BLG is considered a protein relevant for applications as recombinantly produced milk proteins.[20]

In this context, beta-lactoglobulin (BLG) is one of the most relevant proteins, which shows different oligomerization patterns and aggregate contributions upon changes of the solution pH.[21] The targeted BLG aggregation was reported to result in amyloid and amyloid-like aggregates, which is desired for various applications.[22] BLG is a well-characterized model system, which has also been studied with respect to recombinant modification within the amino-acid sequence.[20] BLG monomers, which carry a high charge apart from the isoelectric point, are dominantly present for pH $\leq$ 3 and for pH $>$ 8, otherwise, dimers and higher oligomers, such as octamers, are present.[16] BLG dimers are in equilibrium with monomers as a function of salt concentration, temperature and protein concentration. In case of a sufficient screening or absence of electrostatic interactions, *e.g.* by the addition of ions which suppresses the electrostatic interactions or a change in the solution pH, the formation of hydrogen bonds is enabled, which stabilize the dimer states.[13,21] The monomer–dimer equilibrium of recombinant BLG with a modified N-terminus is not affected by the small changes within the amino-acid sequence since no significant changes of the quaternary structure of the protein were observed.[20]

Monomer–dimer equilibria of BLG can be explained from the PPIs at specific solution conditions. They are described by the interaction potential between macromolecules in aqueous dispersions, *i.e.* by the potential of mean force (PMF). Direct measurement of the PMF and the PPIs contributions is limited. Information about the average effective interactions in a two-body system is provided by the osmotic second virial coefficient B_{22}.[23 25] When considering proteins as spherical particles, B_{22} is related to a PMF as given in eqn (1):

$$B_{22} = \frac{1}{2}\frac{N_A}{M^2}\int_0^\infty \left(1 - e^{\frac{W_{22}(a)}{k_B T}}\right) 4\pi a^2 da \qquad (1)$$

Here, a is the intermolecular center to center distance between two proteins and M is the protein molar mass, $W_{22}(a)$ represents the PMF between two macromolecules. Eqn (1) holds true for dilute systems in which higher order interactions are negligible and higher order virial coefficients can be excluded. Notably, it is possible to formulate a more generalized version of eqn (1), which is introduced within our manuscript.[26]

From a theoretical point of view, the free energy of the salt-dependent binding of BLG can be investigated using molecular dynamics (MD) simulations,[27] but sampling of protein–protein configurations in the total PMF, in eqn (1), beyond the BLG dimer from the crystal structure, was not yet reported. According to the DLVO (Derjaguin, Landau, Verwey, and Overbeek) theory,[28] the PMF consists of the electric double-layer forces and vdW interactions. DLVO theory enables the basic understanding of forces between charged interacting surfaces in aqueous solutions. It has been reported to predict B_{22} in good correlation with available experimental measurements,[9] however, traditional DLVO is an approximate method with a set of limitations.[29] Better description of solution induction effects on the PPIs between proteins was introduced by several post-DLVO theories, *e.g.* reported by Herhut *et al.*[30] or Kastelic *et al.*,[31] known as extended DLVO, *i.e.* xDLVO. Recently, the calculation of the PPIs beyond the spherical-shaped particles, as commonly used in DLVO, was introduced within a xDLVO-coarse-grained (CG) model.[26] Beyond the DLVO theory and the extended models, $W_{22}(a)$ can be estimated using MD and Monte Carlo simulations with both all-atom[32,33] and CG[34] protein representations. The results of these computationally intensive methods have shown that even if the detailed structural and charge characteristics of the protein is properly preserved, other macroscopic features significantly affect the total PMF. Therefore, all-atom simulations are limited for B_{22} predictions and a rescale of the PMFs is necessary.[34]

From an experimental point of view, analytical ultracentrifugation (AUC) is a well-established technique for the analysis of individual macromolecules and (nano-)particles in solution, also with respect to concentration-non-ideality.[11,35,36] From the acquired sedimentation profiles, the sedimentation and diffusion coefficients can be determined for each individual species. From these parameters, the molar mass distribution of the sample is typically retrieved. Moreover, the analysis of the sedimentation profiles allows for a determination of association and dissociation processes for dynamically interacting systems, such as BLG.[14,37] Furthermore, the determination of non-ideality parameters and protein self-association from the analysis of AUC data has already been addressed by the work of Roark and Yphanties.[38,39] Furthermore, recent software developments enabled the direct determination of non-ideality from SV-AUC experiments *via* the software packages SEDANAL[11,40] SEDPHAT.[41]

Membrane osmometry serves as a powerful experimental tool for the determination of osmotic second virial coefficients. However, the reduced osmotic pressure, as measured by membrane osmometry at varying protein loading concentration,[37] is directly affected by the association or dissociation constant of a monomer–dimer system. Thus, the dissociation process must be known in order to study non-specific PPIs (by B_{22}). In this manuscript, we establish a combination of AUC and membrane osmometry as a powerful tool to concurrently characterize both non-specific and specific PPIs for a dynamically interacting system.

For the evaluation of the experimental protocol, the extent of the non-specific PPIs on the BLG monomer–dimer equilibrium as a function of pH and salt concentration is analyzed with a focus on low salt concentration conditions in order to mimic conditions, which are often associated with conditions in food processing.[42] In particular, we determine the extent of specific PPIs in terms of the dimer dissociation constant for the system BLG AB from AUC experiments, a relevant variant of BLG in food technology.[20] With the known dissociation constants of BLG, membrane osmometry measurements enable the experimental determination of the molecular weight-corrected osmotic pressure, which provides the second virial coefficients for the BLG monomer–dimer equilibrium. In this way, we establish an experimental protocol for the determination of PPIs for a system with a concentration-dependent monomer dimer equilibrium.

In order to support the experimental study with theoretical predictions, the osmotic second virial coefficients are calculated using the recently reported xDLVO-CG method, with CG representation of the protein.[26] xDLVO-CG calculations aim to estimate the impact of non-specific interactions in BLG monomer–dimer equilibria. Moreover, we relate the experimentally measured dimer dissociation constant, which is directly converted to the Gibbs free energy, to the extent of non-specific PPIs, *i.e.* the extent of electrostatic interactions. This is further supported by the free energy calculations of the BLG system using MD simulations in combination with an umbrella sampling approach. Finally, based on our results from the experimental protocol, we aim to provide a qualitative prediction for controlled protein oligomerization through the osmotic second virial coefficient.

Theoretical background

Dimer dissociation

Dimer dissociation is usually described by a chemical reaction of second order. Thus, a monomer–dimer equilibrium is modelled according to:[20,37]

$$A_2 \underset{k_b}{\overset{k_f}{\longleftrightarrow}} 2A \tag{2}$$

The dimer and monomer are denoted as A_2 and A. The reaction constants for the forward and backward reaction are denoted k_f and k_b. These finally lead to the dimer dissociation constant K_D, which is provided by the ratio of the reaction constants and the concentrations of the monomer and dimer A and A_2, respectively, according to:

$$K_D = \frac{k_f}{k_b} = \frac{[A]^2}{[A_2]} \tag{3}$$

Here, the monomer and dimer concentration [A] and [A_2] are provided in molar concentrations, *i.e.* mol m ^{3}.

Fundamentals of analytical ultracentrifugation

The sedimentation coefficient is defined as the velocity u acquired by a particle in a centrifugal field $\omega^2 r$ and is given by:[35]

$$s = \frac{u}{w^2 r} = \frac{m_P(1 - \bar{\nu}\rho_S)}{f} \tag{4}$$

The mass of the sedimenting species is denoted as m_P with its partial specific volume $\bar{\nu}$ and translational friction coefficient f. The solvent density is denoted ρ_S. The diffusion coefficient of a protein or particle is described by the Stokes–Einstein relation. For known hydrodynamic diameter x_H, the diffusion coefficient is given by:[43]

$$D = \frac{k_B T}{f} = \frac{k_B T}{3\pi\eta x_H} \tag{5}$$

The Boltzmann constant is denoted as k_B, the temperature as T and the solvent viscosity is η. The evolution of particle concentration c in a sector shaped-centrifugal cell is described by Lamm's equation, which is applied to evaluate the measured sedimentation profiles, from which the sedimentation coefficient and the diffusion coefficient distribution are determined. Lamm's equation is derived from a mass conservation approach taking into account the sedimentation flux and the local diffusive flux and is given by:[36]

$$\frac{\partial c}{\partial t} = D\left(\frac{\partial^2 c}{\partial r^2} + \frac{1}{r}\frac{\partial c}{\partial r}\right) - \omega^2 s\left(r\frac{\partial c}{\partial r} + 2c\right) \tag{6}$$

The radial position within the centrifugal cell is denoted as r and the angular rotor velocity is ω.

Concentration-dependent sedimentation and diffusion coefficient

In the case of moderate and high molar concentrations, the translation friction coefficient has shown to be concentration-dependent.[44,45] This directly translates into a concentration-dependent sedimentation coefficient $s(c)$, which is calculated according to:[46]

$$s(c) = \frac{s^0}{1 + k_s c} \tag{7}$$

The sedimentation coefficient at infinite dilution is s^0. The Gralen coefficient k_s is an empirically introduced constant. Furthermore, the (protein) mass concentration is provided in units of kg m ^{3}. Apart from hydrodynamic effects, the thermodynamic contribution must be considered. In

particular, the virial expansion of the reduced osmotic pressure is provided by:[11]

$$\frac{\Pi}{RTc} = \frac{1}{M}\left(1 + B_{22}Mc + O\left(c^2\right)\right) \tag{8}$$

M is the molar mass of the species with the osmotic pressure Π. The universal gas constant is R. The second virial coefficient is denoted as B_{22}, which accounts for concentration non-ideality. In the context of our results, we apply the second virial coefficient in order to account for non-specific protein–protein interactions. It can be pointed out that the entire protein–protein interactions in solution determine the value of the second virial coefficient B_{22}, which has positive values for globally repulsive protein–protein interactions and negative values in the case of global attraction.[45] Higher order terms are referred to as $O(c^2)$ and take into account non-linear effects including second order and higher terms. These effects are typically observed at high molar concentrations.[11] At higher protein molar concentrations, higher-order terms are required in order to describe non-linear effects such as particle agglomeration[47,48] and cluster sedimentation.[49] Moreover, the ideal contribution of the osmotic pressure of the solution is proportional to the number of molecules in solution, which is linked related to the dimerization constant, which has been introduced in eqn (3). The relationship between these two phenomena describe a central aspect of this manuscript.

From eqn (8), a concentration-dependent diffusion coefficient $D(c)$ can be derived:

$$D(c) = D^0\frac{1 + 2B_{22}Mc - \bar{v}c + O\left(c^2\right)}{1 + k_s c} \tag{9}$$

A detailed derivation of eqn (9) from eqn (8) is provided in literature.[6] The diffusion coefficient at infinite dilution is D^0. Furthermore, there are thermodynamic approaches to account for the presence of protein oligomers during SV-AUC experiments for a defined number of species (*e.g.* dimeric and trimeric oligomers of a protein) in solution.[45,50] Correia *et al.* showed the analysis of SV-AUC experiments with respect to concentration-dependent sedimentation and diffusion coefficient and expressed the interactions constants as matrices, with elements $k_{s,ij}$ and $B_{22,ij}$.[50] The individual terms represent self-interactions (diagonal matrix elements) and cross-correlations (non-diagonal matrix elements) between the individual defined species. In the case of two species in solution (*i.e.* monomers and dimers), the concentration-dependent sedimentation coefficient $s_1(c)$ of the first species is written as:[50]

$$s_1(c) = \frac{s_1^0}{1 + k_{s,11}c_1 + k_{s,12}c_2} \tag{10}$$

The sedimentation coefficient at infinite dilution of the first species is s_0^1. The mass concentration of the two individual species are denoted c_1 and c_2, respectively. Furthermore, the respective concentration-dependent diffusion coefficient $D_1(c)$ is expressed as:[50]

$$D_1(c) = D_1^0\frac{\left[1 + 2B_{22,11}M_{P,1}c_1 + 2B_{22,12}M_{P,2}c_2\right]}{1 + k_{s,11}c_1 + k_{s,12}c_2} \tag{11}$$

The diffusion coefficient at infinite dilution of the first species is D_1^0. The molar masses of the two individual species are denoted as $M_{P,1}$ and $M_{P,2}$, respectively.

Second virial coefficient from membrane osmometry measurements

The molar mass in eqn (8) depends on the degree of dimerization in a monomer–dimer equilibrium system like BLG, and can be represented by:

$$\frac{1}{M} = \frac{w_M}{M_M} + \frac{w_D}{M_D} = \frac{1 - w_D}{M_M} + \frac{w_D}{M_D} \tag{12}$$

Here, w_M and w_D are the weight fractions and M_M and M_D represent the molecular mass of the monomer and the dimer, with $M_M = 0.5M_D$ and $w_M = 1 - w_D$. If the concentration is sufficiently low and higher order interactions can be neglected, the reduced osmotic pressure of a monomer–dimer system is given by:[51]

$$\frac{\Pi}{RTc_w} = \frac{1}{1 + w_D M_D} + B_{22}c_w \tag{13}$$

The weight concentration of the protein is denoted c_w. According to Schaink and Smit (2000),[52] the weight fraction w_D for an ideal protein solution is given by:[51]

$$w_D = 1 + \frac{M_D K_D}{8c} - \sqrt{\left(\frac{M_D K_D}{8c} + 1\right)^2 - 1} \tag{14}$$

By insertion of eqn (14) into eqn (13) and correcting for the reduced osmotic pressure by subtracting the molecular weight-dependent term in eqn (13), B_{22} can be determined in the case of known osmotic pressure and dissociation constant K_D. When the molecular weight corrected osmotic pressure is plotted against the protein concentration, a straight line is obtained with a y-intercept at zero protein concentration. The slope gives B_{22}.

As stated before, if there is more than a single species in the solution, the second virial coefficient is associated with several contributions, namely self-interaction as well as cross-correlations. This could already be seen in eqn (11) and links this equation to eqn (8), (12) and (13). In the case of membrane osmometry, a single value for the osmotic second virial coefficient B_{22} from a concentration-dependent and molecular weight-corrected osmotic pressure is obtained from eqn (13), which includes all contributions from monomer–monomer interactions B_{MM} and dimer–dimer interactions B_{DD} as well as monomer–dimer interactions B_{MD}.[8,11,14,50] In the case of a monomer–dimer system, the second virial coefficient consists of all contributions according to:

$$\begin{aligned} B_{22} &= \frac{B_{MM}}{M_M{}^2} + 2\left(\frac{B_{MD}}{M_M M_D} - \frac{B_{MM}}{M_M{}^2}\right)w_d \\ &\quad + \left(\frac{B_{MM}}{M_M{}^2} - 2\frac{B_{MD}}{M_M M_D} + \frac{B_{DD}}{M_D{}^2}\right)w_D{}^2 \end{aligned} \tag{15}$$

Combining eqn (13) and (15) leads to an expression for the reduced osmotic pressure in a monomer–dimer system according to:[53]

$$\frac{\Pi}{RTc_w} = \left(\frac{1-w_D}{M_M}+\frac{w_D}{M_D}\right)+\left[\frac{B_{MM}}{M_M{}^2}+2\left(\frac{B_{MD}}{M_M M_D}-\frac{B_{MM}}{M_M{}^2}\right)w_D + \left(\frac{B_{MM}}{M_M{}^2}-2\frac{B_{MD}}{M_M M_D}+\frac{B_{DD}}{M_D{}^2}\right)w_D{}^2\right]c_w \quad (16)$$

Interaction potential from xDLVO-CG calculations

In the present study, we use a recently reported extended DLVO approach, *i.e.* xDLVO-CG,[26] for the interaction potential $W_{22}(a)$ (see eqn (1)) between BLG monomers and dimers. The BLG protein and protein oligomers are represented by the shape-based CG model, which is visualized in Fig. 1, $W_{22}(a)$ is calculated as a sum of electrostatic, $W_{el}(a)$, dispersion, $W_{disp}(a)$, osmotic, $W_{osm}(a)$ and ion–protein $W_{i\ prot}(a)$, interactions between the BLG monomers and dimers binary systems:

$$W_{22}(a) = W_{el}(a) + W_{disp}(a) + W_{osm}(a) + W_{i\ prot}(a) \quad (17)$$

Electrostatic interactions are calculated within DLVO theory[28,54] using Debye–Hückel theory,[55] to account for interparticle interactions in the presence of electrolytes:

$$W_{el}(a) = \sum_{i=1}^{N_1}\sum_{j=1}^{N_2}\frac{Z_i Z_j e^2 e^{\kappa(d_{ij}\ \ a_{ij})}}{4\pi\varepsilon_0\varepsilon_r a\left(1+\frac{\kappa d_{ij}}{4}\right)^2}, \quad a_{ij} > d_{ij}+2\sigma \quad (18)$$

Here, a is the center-of-mass (COM) distance between two proteins, N_1 and N_2 are the total numbers of CG beads of each protein, d_{ij} is the initial distance between beads i and j when proteins are in starting position, a_{ij} is the current (variable) distance between beads during pulling calculations, σ is the length of water layer around a protein (0.1 nm), ε_r is the relative permittivity, Z_i and Z_j are the charges of each bead and κ is the inverse Debye length, which is given by:

$$\kappa = \sqrt{\frac{2N_A e^2 I}{\varepsilon_0\varepsilon_r k_B T}} \quad (19)$$

I is the ionic strength. The dispersion potential $W_{disp}(a)$, which is used to describe the attraction forces between macroscopic uncharged colloidal particles,[56] is calculated as a result of the summation of vdW interactions between CG beads representing BLG proteins, as can be seen in Fig. 1. Here, these interactions are calculated using the Hamaker constant A_H estimated experimentally (see in Materials and methods):

$$W_{disp}(a) = \sum_{i=1}^{N_1}\sum_{j=1}^{N_2}\frac{A_H}{12}\frac{1}{N_1 N_2}\left[\frac{d_{ij}}{a_{ij}{}^2-d_{ij}{}^2}+\frac{d_{ij}{}^2}{a_{ij}{}^2}+2\ln\left(1-\frac{d_{ij}{}^2}{a_{ij}{}^2}\right)\right], \quad a_{ij} > d_{ij}+2\sigma \quad (20)$$

In addition to the Hamaker-based approach, we calculated B_{22} using the dispersion interactions based on the Lennard-Jones potential between BLG molecules (see Fig. S1-1, ESI†).

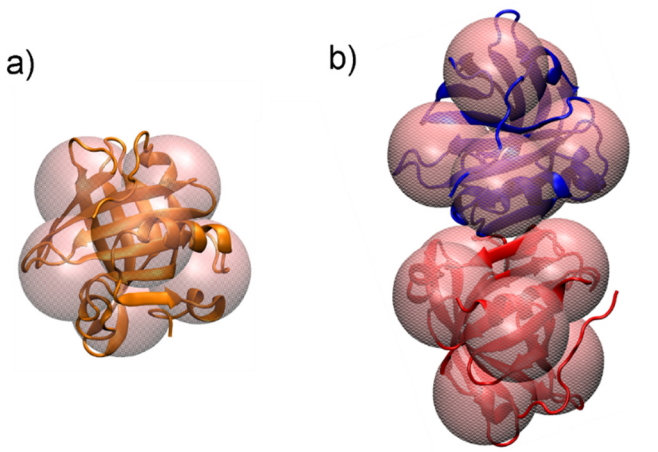

Fig. 1 Coarse-grained representation of BLG monomer (a) and dimer (b) used to calculate the second osmotic virial coefficient B_{22} by means of xDLVO-CG.

The osmotic potential $W_{osm}(r)$ between two proteins due to salt ions exclusion from the protein interspace at short distances, which raises local osmotic pressure imbalance and causes additional attractive interaction between proteins, was calculated according to eqn (21):[57]

$$W_{osm}(a) = \sum_{i=1}^{N_1}\sum_{j=1}^{N_2}\frac{1}{N_1 N_2}\frac{4\pi k_B}{3}TD_{ij}{}^3\rho_3\left(1-\frac{3a_{ij}}{4D_{ij}}+\frac{a_{ij}{}^3}{16D_{ij}{}^3}\right), \quad a_{ij}+2\sigma \le a_{ij} \le 2D_{ij} \quad (21)$$

where D_{ij} is defined by eqn (22) with R_3 as the mean hydrated radius of the salt (taken as a sum of anion and cation radii) and ρ_3 as the salt density:

$$D_{ij} = d_{ij} + R_3 + \sigma \quad (22)$$

The last term in the PMF (eqn (17), *i.e.* the ion–protein potential, describes the total dispersion interaction between protein and all ions in its surrounding. In this model, the protein is represented as an ideal sphere with the charge Z, while ions are placed non-uniformly around the protein sphere according to the Gouy–Chapman model. The total potential is calculated by integrating the contributions of each ion according to:

$$W_{i\ prot}(a) = -4\pi B_{anion}\int_{R_P+\sigma}^{R_P+d}\frac{c_{bulk}e^{\frac{z_{anion}\phi(a)}{k_B T}}}{a}da - 4\pi B_{cation}\int_{R_P+\sigma}^{R_P+d}\frac{c_{bulk}e^{\frac{z_{cation}\phi(a)}{k_B T}}}{a}da \quad (23)$$

where B_{anion} and B_{cation} represent the ion–macroion dispersion coefficients taken from literature,[58,59] R_p is the protein radius, d is the thickness of the spherical shell around a protein, in which ions are placed, z_{cation}/z_{anion} are the charges of the cation/anion, c_{bulk} is the salt concentration and $\varphi(a)$ is the

electrostatic potential around a protein sphere with charge Z calculated from:

$$\varphi(a) = \frac{Z^2 e^2 e^{\kappa(2R_p \quad a)}}{4\pi\varepsilon_0\varepsilon_r a\left(1+\frac{\kappa R_p}{2}\right)^2}, \quad a > 2(R_p+\sigma) \tag{24}$$

Notably, throughout our xDLVO calculations, salt specific ion–macroion dispersion coefficients are taken in order to calculate ion–protein dispersion interaction of ions around proteins as a function of protein COM distance. This is in accordance with approaches taken in literature.[58,60 64]

The second osmotic virial coefficient between the BLG monomers and dimers was calculated for different sampled configurations by the numerical integration of the average PMF according to eqn (25):

$$B_{22} = \frac{1}{16\pi^2}\frac{N_A}{M^2}\int_0^{2\pi}\int_0^{\pi}\int_0^{2\pi}\int_0^{2\pi}\int_0^{\pi}\int_0^{\infty}\left(e^{\frac{-W}{k_B T}}-1\right) r_{12}^2 dr_{12} \times \sin(\theta)d\theta d\phi d\alpha d\beta d\gamma \tag{25}$$

Here, Euler angles α, β and γ specify orientation and φ and θ angles specify angular orientation of the second protein with respect to the first protein, which is placed at the center of coordinate system. M denotes molar mass of the protein, *i.e.* of two BLG monomers, of one monomer and one dimer, and of two dimers for B_{MM}, B_{MD} and B_{DD}, respectively. According to the reconstructed structure of the BLG (3ph5 code) as described in the materials and methods, molar mass of BLG monomer of 18 182 g mol ^{1} and 18 156 g mol ^{1} was used for BLG at pH 3 and pH 7, respectively.

Materials and methods

Coarse-grained molecular calculations

The original DLVO model accounts for electrostatic and vdW interactions between two charged spherical particles. To gain an impact of other non-specific PPIs and to account for the differences in the charge distribution over the protein, we used a CG representation of monomeric BLG and its oligomers, which is visualized in Fig. 1.

The all atom structure of BLG was taken from the protein data bank with the 3ph5 code.[65] The chosen structure contains two BLG units placed in a crystallographic cell, which was taken to represent the BLG dimer. Both protein units have several missing residues (chain A: ILE 18, VAL 19, TYR 115, LYS 117, chain B: VAL 19, THR 20, GLN 21, THR 22, ASP 49). They were modeled by Swiss Model program.[66] The reconstructed structures were protonated at pH = 3 and pH = 7 using PROPKA method[67] (version 3.3) and PDB2PQR online webserver.[68] This resulted in the charge of the BLG monomer of +18e and −8e [69] at pH 3 and pH 7, respectively (while experimentally determined charges are +20e at pH 2.5 and −9e at pH 7.5).[69] The reconstructed and protonated all-atom structures were used to map the BLG into the CG representation (Fig. 1; variant BLG-A). One CG bead equals to approximately 500 atoms of a protein (6 and 12 beads for the BLG monomer and dimer, respectively) with the center of the bead placed in the COM of atoms, which constitute each bead, estimated by the neural network algorithm[70] within the shape-based CG model, implemented in VMD program (version 1.9.3).[71] Each bead has a charge equal to the sum of atomic charges, therefore depends on the specific protonation state of the BLG residues represented by a bead. Eqn (20)–(25) were calculated by summing interactions between the corresponding bead pairs from both CG-proteins. The PMF and the corresponding B_{22} were calculated by the in-house code. Calculations were performed for BLG monomers, dimers and mixtures at pH 3 and pH 7 with salt concentrations of 10 mM and 100 mM sodium chloride. A Hamaker constant of $5.1k_BT$ was taken from experimental data to calculate the dispersion potential.[17]

B_{22} was calculated by numerical integration of the average PMF according to eqn (25) and the procedure described by Pusara *et al.*[26] Conformational sampling of starting protein–protein configurations was done performing 16 different rotations at each of the 83 starting radial positions, resulting in 1328 starting configurations. Each of them was used for a separate PMF calculation based on pulling one BLG protein along a vector connecting the COM of the second BLG protein. The PMF up to a COM distance of 30 nm was calculated. Finally, B_{22} was calculated using an average of all PMFs, which corresponds to averaging along all different configurations (eqn (25)).

Umbrella sampling simulations

Umbrella sampling simulations (US) between BLG monomers at studied experimental conditions were performed using the CHARMM36m force field[72] and SPC water model[73] as implemented in the GROMACS package (version 2019.2).[74] All calculations were performed using periodic boundary conditions with a rectangular box of the size 18.0 × 9.5 × 9.5 nm^3, where the BLG monomers were aligned to the x-axis with respect to their center to center distance vector. Structures of the reconstructed and protonated BLG proteins, as discussed before, were charge neutralized and used in all further simulations. Hydrogen atoms at specific pH were added according to PROPKA method[49] (version 3.3) and PDB2PQR online webserver. Protein protonation states at specific pH were assigned by PROPKA method[49] (version 3.3) and PDB2PQR online webserver. Na^+ and Cl ions were added to fulfill salt concentrations of 10 mM and 100 mM, used in the experiments. All systems were initially minimized by the steepest descent algorithm during 30.000 steps with position restraints applied to proteins heavy atoms. Equilibration under canonical (*NVT*) and later under constant–pressure (*NPT*) ensembles at 300 K and for 400 ps per each were performed using Berendsen thermostat.[75] The Berendsen weak coupling method was also used to isotropically maintain pressure at 1.0 bar. All simulations were performed with the timestep of 2 fs. Short-range nonbonded interactions were cut off at 1.2 nm. The full electrostatic interactions beyond

1.2 nm were evaluated by the particle mesh Ewald (PME algorithm).[76]

To optimize the US setup, pulling simulations along the *x*-axis for 1.2 ns using the spring constant of 1000 kJ (mol nm^2)$^{-1}$ and a pull rate of 0.005 nm ps^{-1} were performed. This set-up was applied for all BLG systems except for a solution pH of 3 and a salt concentration of 100 mM sodium chloride. Here, the spring constant was 1500 kJ (mol nm^2)$^{-1}$. Proteins were pulled from their starting position (COM distance of 3 nm) up to a COM distance of 8.5 nm. The snapshots from the collected pulling trajectories were used to generate starting configurations for the respective US windows. An asymmetric distribution of sampling windows was used: the window spacing of 0.0625 nm (or smaller) and 0.125 nm was used for COM distances shorter than 4.1 nm and longer than 4.2 nm, respectively. In total, 61 US windows were generated. In each window, the system was equilibrated using *NPT* ensemble at 300 K and 1 bar for 400 ps with the following 20 ns MD run using *NPT* ensemble with Nosé–Hoover thermostat[77] and Parrinello–Rahman barostat.[78] Analysis of all US simulations was performed with the weighted histogram analysis method (WHAM).[79]

Beta-lactoglobulin

BLG AB was isolated from bovine whey protein isolate (Bipro, Agropur Diary Cooperative Inc., Minnesota, USA). The protein was isolated according to the method described by Keppler *et al.*[80] with slight modifications. The ultrafiltration was replaced by dialysis against distilled water for 3 days using BioDesignDialysis Tubing™ (Thermo Fischer Scientific, Waltham Massachusetts, USA) with a molecular weight cut-off of 14 kDa. Prior to freeze-drying, the solution was adjusted to a pH of 7 using 100 mM HCl and 100 mM NaOH (Carl Roth GmbH, analytical-grade, Karlsruhe, Germany). The resulting protein powder consisted of 97.6% native BLG, 2.0% denatured BLG and 0.4% α-lactalbumin as measured by HPLC according to Keppler *et al.*[80] According to the reconstructed structure of the BLG (3ph5 code), the molar mass of BLG monomer is 18 182 g mol^{-1} and 18 156 g mol^{-1} at pH 3 and pH 7, respectively.

Protein sample preparation for analytical ultracentrifugation experiments

For the determination of the dissociation constant K_D, concentration series of BLG were measured by analytical ultracentrifugation. BLG was investigated at a solution pH of 3 and 7 at salt concentrations of 10 mM and 100 mM sodium chloride (≥99.8%, Carl Roth GmbH, Karlsruhe, Germany), respectively. Prior to dilution, a highly concentrated BLG stock solution with a protein concentration of 1000 μM was prepared at a fixed solution pH and salt concentration and dialyzed against 600 mL of a solution with the same solution pH and salt concentration to ensure constant ionic strength within each protein concentration series. Following the protocol by Schuck *et al.*,[81] the dialysate was changed after 6 hours and dialysis was continued overnight. Afterwards, the BLG stock solution was filtered using syringe filters with 0.2 μm pore size and a 1 : 20 dilution was prepared subsequently. The filtered stock solution concentrations were determined *via* UV-Vis spectrometry using a specific extinction coefficient of 17 679 cm M^{-1}, which was determined beforehand for a wavelength of 280 nm (see Fig. S2, ESI†). Protein concentrations between 0.25 μM and 500 μM were prepared *via* dilution and measured again with UV-Vis spectrometry to confirm the protein concentration. In order to ensure a constant ionic strength within the protein dilution series, all protein samples were diluted with the respective dialysate. The pH was adjusted to the desired value by adding HCl (0.1 M Honeywell™ Fluka™, Thermo Fisher Scientific Inc., Schwerte Germany) or NaOH (0.1 M Merck KGaA, Darmstadt, Germany). All solutions were prepared in deionized Millipore water with a resistivity of at least 17 MΩ cm.

Analytical ultracentrifugation experiments

For all sedimentation velocity (SV) experiments, a commercial ultracentrifuge, type Optima™ AUC from Beckman Coulter (Krefeld, Germany), was used. The samples were measured at a fixed rotor speed of 40 000 rpm or 50 000 rpm for 10 hours until complete sedimentation of all species was observed. The temperature was kept constant at 20 °C. Depending on the sample and preparation, the wavelength was adjusted in order to obtain the optimal signal during the SV experiment. SV experiments were conducted using centerpieces with an optical path length of 12 mm or 3 mm in order to adjust the optical signal. When converting intensity data to absorbance data, pseudo-absorption of each sample was calculated and analyzed as described by Kar *et al.*[82] Following the protocol by Schuck *et al.*,[14,81] SV data was first analyzed with the continuous *c*(*s*) model which is implemented in the SEDFIT software (Version 16-1c).[36] The sedimentation coefficient distributions and the weight-averaged sedimentation coefficients for varying protein concentrations were determined using the partial specific volume of 0.751 mL g^{-1} for BLG as calculated from Sednterp.[83] The solvent density and viscosity were set to the values of the solution at the respective salt concentrations at 20 °C. Determination of the dimer dissociation constant was subsequently conducted *via* fitting the isotherms, *i.e.* weight-averaged sedimentation coefficient for varying protein concentration at a fixed pH value and salt concentration, using the software SEDPHAT and following the protocol of Zhao *et al.*[14,81]

Protein sample preparation for membrane osmometry experiments

For membrane osmometry measurements, BLG stock solutions with a protein powder content of 40 g L^{-1} were prepared in 10 mM and 100 mM sodium chloride solution at pH 3 and pH 7. The stock solutions were stirred for 1 h and stored in a refrigerator overnight. The samples were diafiltered (ÄKTA-Crossflow™, GE Healthcare, Uppsala, Sweden) for precise adjustment of the ionic strength and the pH value. The volume of the stock solution was exchanged 10 times with the corresponding, pH adjusted sodium chloride solution. The diafiltration was performed according to Hundschell *et al.*[51] To remove any potential protein aggregates, the diafiltered samples were centrifuged for 30 min at 4 °C and 10 000*g*. The residue was

discarded and the protein concentration of the supernatant was determined by measuring the absorbance at 278 nm with a Helios Omega UV-vis spectrophotometer (Thermo Fisher Scientific, Waltham Massachusetts, USA) using a specific extinction coefficient of 0.96 L (g cm) ^{1}.

Membrane osmometry experiments

Osmotic pressure measurements were performed at various protein concentrations as previously described by Hundschell *et al.*[51] The osmotic second virial coefficient was determined using eqn (12)–(14).

Results and discussion

Coarse-grained molecular B_{22} calculations

PPIs between the BLG (BLG-A) monomers and dimers are highly modulated by the solution pH, resulting in the total charge per monomer (PROPKA method) of +18*e* and −8*e* at pH 3 and pH 7, respectively. The dimer binding site of BLG, stabilized by several H-bonds (often five),[21] is schematically depicted in Fig. 2. It is seen that this part of BLG is highly positively charged at pH 3, therefore, an assembly into dimers without any salt addition is not possible. This is changed after an increase of the salt concentration, which is analyzed subsequently. The interaction potential (see eqn (17), which we calculated to derive B_{22}, consists of several potentials. Fig. 3 depicts the contribution of the electrostatic and the dispersion interactions at different pH values and salt concentrations to the overall interaction potential. We see the highest contribution of the electrostatic repulsion, which drops down significantly when increasing the salt concentration from 10 mM to 100 mM sodium chloride, especially at pH 3. Strong reduction of the repulsion occurs at higher salt concentration and upon increasing the solution pH. At the same time, the strength of the dispersion interactions, calculated using the Hamaker constant (see eqn (20) and the Lennard-Jones potential (see Fig. S1-1, ESI†) is one order of magnitude lower, suggesting the dominant role of the non-specific electrostatic interactions between the BLG proteins.

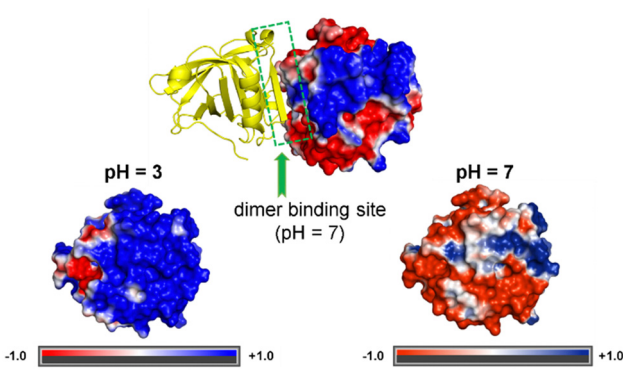

Fig. 2 Graphical representation of the charge state of the BLG monomer and dimer as a function of the solution pH. The dimer binding site is indicated. The electrostatic potential was calculated using an Adaptive Poisson–Boltzmann Solver (APBS)[84] with a default grid dimension, as implemented in the APBS software.

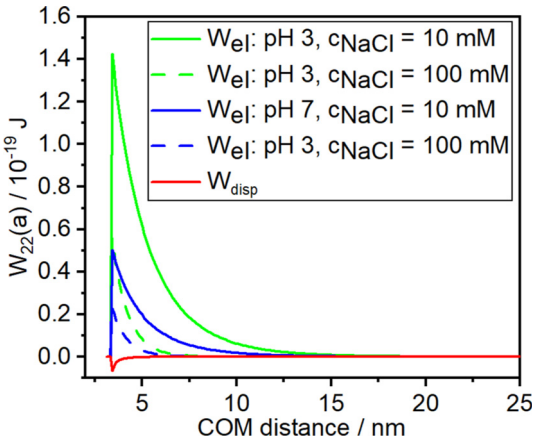

Fig. 3 Interaction potential $W_{22}(a)$ as a function of the protein–protein COM distance. The electrostatic interaction potential (W_{el}) is shown for a salt concentration of 10 mM sodium chloride (solid lines) and 100 mM sodium chloride (dashed lines) at pH 3 (in green) and pH 7 (in blue) alongside the contribution from dispersion interactions (marked in red).

Similar trends were also observed in the case of the monomer–dimer and dimer–dimer interactions. This observation is in line with the reported change of the PMF upon increase of the salt concentration, which was shown by MD simulations in combination with a Reference Interaction Site Model three-dimensional (3D-RISM) solvent model.[27]

The contribution of the ion–protein interactions and the osmotic-pressure imbalance, *i.e.* osmotic potential, to the PMF at low salt concentrations, as are used in the present study, are negligible. The strength of these potentials is in the range of ~10 ^{23} J and 10 ^{22} J at salt concentrations of 10 mM and 100 mM sodium chloride, respectively. The local density distribution and binding of Cl anions by charged residues, responsible for the charge screening of the positive charge of BLG at pH 3, was shown by Srivastava *et al.*[27] Finally, upon an increase of the solution pH and the ionic strength, the surface charge of the BLG protein changes (see Fig. 2), which causes different PPI patterns and the interplay between non-specific and specific interactions. Moreover, there is a further change of the ratio between electrostatic repulsion and attractive vdW forces. The theoretically calculated values for B_{22} can be seen in Fig. 4.

The dependence of B_{22} on the salt concentration within the BLG system is slightly different for monomer–monomer, monomer–dimer and dimer–dimer interaction (with a larger difference at pH 3). However, all B_{22} values at salt concentrations of 10 mM and 100 mM sodium chloride are rather similar, indicating an equilibrium state. Notably, both monomers and dimers tend to bind Cl ions by the charged residues with the same affinity,[27] resulting in the similar mechanism of the screening the electrostatic repulsion. The values for B_{22} are listed in Table S1 (ESI†). In Fig. 4(a and b), we observe the typical decrease of B_{22} upon increase of the salt concentration, as the electrostatic repulsion is screened and the attraction between BLG monomers drives the dimer formation. However,

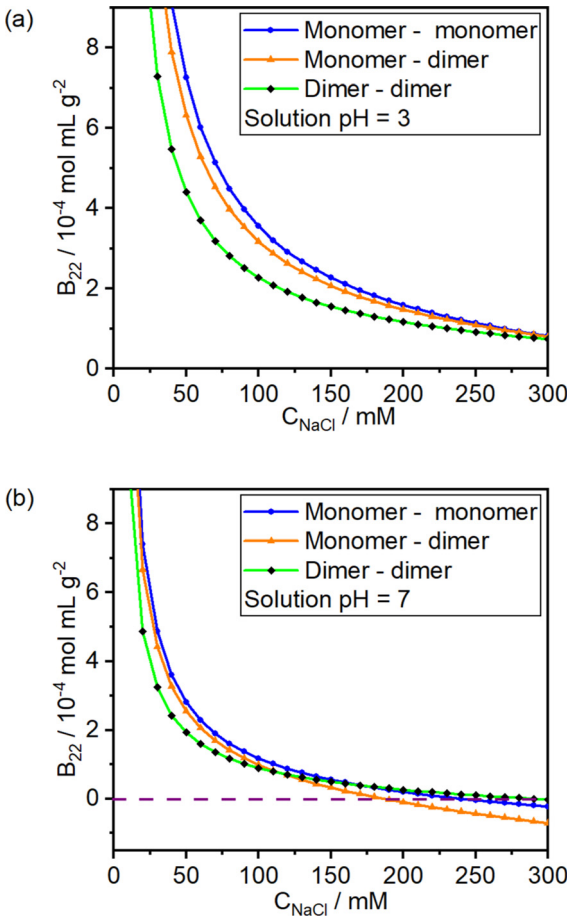

Fig. 4 Osmotic second virial coefficient B_{22} as calculated using xDLVO-CG for BLG monomer–monomer, monomer–dimer and dimer–dimer interactions as a function of the salt concentration at pH 3 (a) and at pH 7 (b).

all B22 values at salt concentrations of 10 mM and 100 mM sodium chloride are rather similar, indicating similar strength of non-specific interactions between monomers and dimers. Moreover, the decrease of B_{22} as a function of the ionic strength is significantly steeper at pH 7, promoting protein assembly. This is caused by the differently charged states of BLG with a lower contribution from repulsion. Due to the lower BLG charge at pH 7, hence reduced repulsion screening, we further observe B_{22} values ~ 0 mol (mL g^2)$^{-1}$ at higher sodium chloride concentrations at pH 7. This does not occur at pH 3 due to the lower BLG charge at pH 7 and, hence reduced repulsion screening. Values of B_{22} for BLG monomers, dimers and mixtures are rather similar at pH 7 and pH 3.

A traditional DLVO approach lacks the adequate charge distribution over a spherical particle (one protein–one particle with a point charge). It should be noted that the traditional DLVO approach overestimates the second virial coefficients of all species considered by a factor of *ca.* 1.5–2.5 at pH 3 and even by a factor of 3 at pH 7 (see Fig. S1-2, ESI†) due to the lack of adequate charge distribution and anisotropy over a spherical particle (one protein–one particle with a point charge) that is accounted for in xDLVO-CG calculations (see Fig. S1-3, ESI†). All-atom and coarse-grained MD simulations overestimate protein–protein binding affinities.[27] Finally, within this manuscript, we provide a detailed insight into the nature of PPI interactions and develop a methodology to quantify non-specific interactions as well as their impact on the specific PPIs. So far, the extent of non-specific interactions was theoretically quantified using an xDLVO-CG approach. Our simulations revealed a strong dependence of the non-specific interactions on the electrostatic properties, as has been demonstrated in Fig. 3 and 4. Moreover, the chemical nature of the dimer binding site was demonstrated.

Dimer dissociation constant from analytical ultracentrifugation experiments

For the determination of the dimer dissociation constant *via* AUC experiments, a BLG concentration series was prepared for each solution pH (pH 3 and pH 7) and salt concentration (10 mM and 100 mM sodium chloride). For each combination of solution pH and buffer concentration, the sedimentation and diffusion properties were determined from SV-AUC experiments.

Sedimentation profiles for a solution pH of 7 and a salt concentration of 100 mM sodium chloride with a BLG concentration of 55 μmol L^{-1} are provided in Fig. 5(a). Sedimentation coefficient distributions for the BLG system for a solution pH of 7 at different protein loading concentrations are shown in Fig. 5(b). The presence of sedimentation non-ideality[45] is already visible in the data and indicated by minor shifts in the sedimentation coefficient distribution at different BLG concentration, as can be seen in Fig. 5(b). Moreover, a shift of the ratio of BLG monomers to dimers becomes obvious from the plot in Fig. 5(b), depending on the BLG loading concentration. Notably, sedimentation coefficient distributions for the BLG system for a solution pH 3 and 7 at different salt concentrations are shown in the left panel of Fig. S3 (ESI†) in order to illustrate the pH and salt concentration dependence of the dimer dissociation.

Following the protocol by Schuck *et al.*,[81] all SV-AUC data sets were analyzed with respect to the weight-averaged sedimentation coefficient. For a fixed solution pH and salt concentration, the weight-averaged sedimentation coefficient as a function of the BLG loading concentration provides the monomer–dimer equilibrium. Each isotherm, *i.e.* weight-averaged sedimentation coefficient for various protein concentrations,[81] contains information about the dissociation of the dynamically interacting system. Determination of the dimer dissociation constant K_D was subsequently conducted *via* fitting the isotherms using the software SEDPHAT.[14] Notably, the dissociation constant is directly linked to the dissociation energy, which will be discussed in a later section of this manuscript. Notably, during the data analysis in SEDPHAT, we kept the value of k_s constant at a value of 10 mL g^{-1}, which reflects the excluded volume for globular proteins.[81] Moreover, in order to test the influence of hydrodynamic interactions on the retrieval of the dimer dissociation constant K_D, we treated the Gralen coefficient k_s as a floating parameter during the analysis in SEDPHAT.

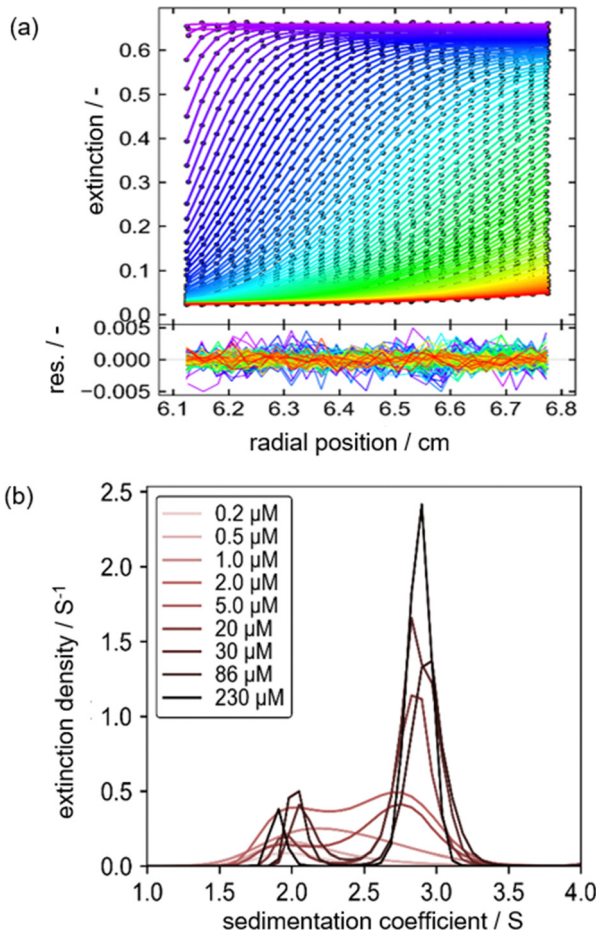

Fig. 5 (a) Exemplarily measured sedimentation profiles as obtained from AUC experiments for a solution pH of 7 and a salt concentration of 100 mM sodium chloride and a protein concentration of 18 μmol L^{-1}. Data acquisition was carried out at a wavelength of 280 nm. The color code indicates the course of the sedimentation profile over time.[85] (b) Retrieved sedimentation coefficient distributions for BLG in water at pH 7 and a salt concentration of 100 mM sodium chloride at various protein loading concentrations. The sedimentation data was analyzed using the *c*(*s*) model.[14] The plot was created using GUSSI.[85]

We found for the concentration range within the isotherms no significant difference from the value reflecting the excluded volume.[81] Almost identical values for the dissociation constant K_D were retrieved from the analysis with floating and constant k_s. Therefore, we continued the determination of the dissociation constant with a constant value for the Gralen coefficient.

Moreover, the influence of hydrodynamic non-ideality further explain the minor difference between the fitted isotherm and the measured data at elevated protein concentrations, as the influence of hydrodynamic non-ideality increases at higher protein concentrations. Finally, our experimentally determined isotherms are graphically shown in Fig. 6 for a solution pH of 3 and 7 at a salt concentration of 100 mM sodium chloride and a solution pH of 7 at a salt concentration of 10 mM sodium chloride. Notably, the measured isotherm at a solution pH of 3 and a salt concentration of 10 mM sodium chloride did not follow the expected trend (see right panel of Fig. S3, ESI†). Consequently, we were not able to analyze this isotherm with respect to K_D. This observation is attributed to a significant influence of the primary charge effect throughout the AUC experiments, which can be explained as follows. The difference in sedimentation velocity of charged particles and their respective counter ions is the origin of the primary charge effect. This effect is more important for technical conditions at a low ionic strength, which is the case for our system at a salt concentration of 10 mM sodium chloride.[14,86] In the context of our results, the total number of charges in the system are determined by the BLG loading concentration as the charge screening is significantly reduced at the salt concentration of 10 mM sodium chloride. Thus, the influence of the primary charge effect scales with the BLG loading concentration, which makes analysis of the weight-averaged sedimentation coefficient for varying protein loading concentration with respect to dimer dissociation impossible at a solution pH of 3 and a salt concentration of 10 mM sodium chloride, as can be seen in the right panel of Fig. S3 (ESI†).

The dimer dissociation constants for the three other solution conditions were analyzed and the retrieved values are provided in Table 1. Notably, the confidence intervals for the calculation of the error bars were set to 68%: the statistical errors were calculated using Monte Carlo simulations based on the provided confidence interval. From the plot, it can be taken that the dimer dissociation depends on the solution pH, which is directly in line with a previous AUC study on genetically modified BLG systems.[20] While dimers predominantly form at pH 7, dimer dissociation is stronger at pH 3. This is further in agreement with the results from Mercadante *et al.*[87] In this work, it was shown how the BLG dimerization is significantly influenced by the buffer type and concentration over a broad range of solution pH values. As already pointed out, the dimer dissociation is further influenced by the ionic strength, which is caused by the strong modulation of PPIs, necessary for subsequent dimerization, and by the charge state of the protein. This can further be related to the protein CG model in Fig. 2, which indicated a high charge density at the dimer binding site. In this context, Gottschalk *et al.*[16] studied the salt-dependent monomer–dimer equilibrium and revealed a significant difference between no addition of salt and a 1 M sodium chloride solution. The authors show an essentially monomeric state in the absence of salt and a solution pH of 2.5 while dimerization is observed at a salt concentration of 1 M sodium chloride.[16]

Notably, it was not possible for the investigated range of concentrations by AUC to retrieve the osmotic second virial coefficient directly from experimental data, hence we restrict our AUC analysis of the BLG system to the retrieval of the dimer dissociation constant and exclude the determination of the second osmotic virial coefficient with respective self and cross-term interactions (see *e.g.* eqn (10) and (11)). This is attributed to the fact that we experimentally investigate a mixture of two BLG variants (A and B), since BLG is considered a relevant protein in food technology as a milk protein.[20]

Therefore, while the number of self-interaction terms significantly increases (*e.g.* A–A, AA–AA, B–B, AB–AB, *etc.*), the cross-term interactions in eqn (10) and (11) would involve at

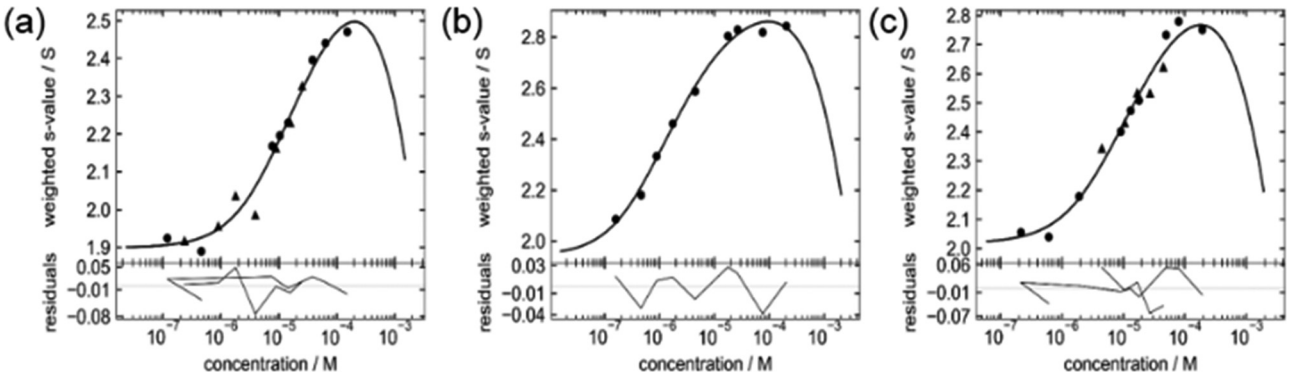

Fig. 6 Weight-averaged sedimentation coefficients as measured by AUC experiments *versus* BLG loading concentration. The isotherms are determined for different solution conditions: (a) pH 3 with a salt concentration of 100 mM, (b) pH 7 with a sodium chloride concentration of 100 mM and (c) pH 7 at a salt concentration of 10 mM sodium chloride. Each isotherm is fitted using the software SEDPHAT in order to determine the dimer dissociation constant. Notably, beyond protein concentrations of 10^{-4} M, the influence of non-ideality phenomena is strongly increased,[11,81] thus extrapolation of the isotherms is not possible and cannot be interpreted in a physical manner.

Table 1 The dimer dissociation constant as obtained from fitting of the isotherms, which are determined from AUC experiments. The dimer dissociation constants are provided as a function of solution pH and salt concentration. At a solution pH of 3 and a salt concentration of 10 mM sodium chloride, the AUC experiments are influenced by charge effects. The values for the dimer dissociation constant based on a confidence interval of 68% are provided

	pH 3		pH 7	
NaCl concentration	10 mM	100 mM	10 mM	100 mM
Dimer dissociation/μM	Strong charge effects	29.2	19.3	2.1
Confidence intervals 68%/μM	NA/NA	27.6/31.2	18.1/20.6	2.1/2.3

least eight terms (*e.g.* A–AA, A–AB, *etc.*). Therefore, it is not possible to analyze these interactions from SV-AUC data when a high number of unknowns are included in additional terms in eqn (10) and (11). Moreover, we point out that the heterogeneity of the species contribute to the broadening of the sedimentation boundary, which directly influences the sedimentation analysis with respect to the second virial coefficient. Notably, the hydrodynamic non-ideality constant k_s remains an effective constant representing the hydrodynamic non-ideality of both, the BLG monomer and the dimer as well as their cross-terms. Furthermore, a recent analysis of self-interaction and cross-term interactions for therapeutic antibodies in a highly concentrated environment *via* SV-AUC experiments by Correia *et al.* has shown that the absolute values of the retrieved individual cross-terms do not show significant variations in direct comparison (variation by 5–10%).[10,50] Such small differences cannot be resolved from our SV-AUC data. In this context, it was further shown that an extensive systematic study *via* SV-AUC over a broad range of protein loading concentrations with different detection systems, such as the Aviv AU-FDS optical system, is required to study the wide range of protein interactions, which eventually provides insight into self and cross-term interactions.[10]

We rely on the determination of the second osmotic virial coefficient from membrane osmometry measurements, which relies on the determination of the dimer dissociation constant from AUC. Our approach aims to establish an experimental protocol for the determination of PPIs for dynamically interacting systems such as the complex system with BLG monomers and dimers. The measured dissociation constant K_D by AUC thus represents the equilibrium of BLG monomers and dimers as defined in eqn (3).

Determination of the osmotic second virial coefficients from membrane osmometry experiments

Following the results from AUC experiments for each combination of solution pH and salt concentration, the reduced osmotic pressure was determined from membrane osmometry measurements for various BLG loading concentrations. Our results are presented in Fig. 7(a). Evidently, the extent of the concentration-dependency varies with the combination of solution pH and salt concentration, thus the nature of the electrostatic properties. The extent of the non-specific interactions was quantified by fitting eqn (13) to the molecular weight corrected reduced osmotic pressure for various BLG loading concentrations, which is only possible in case the dimer dissociation constant is known. For each solution pH and salt concentration, the dimer dissociation constant was taken from Table 1 as measured by AUC. For a solution pH of 3 and a salt concentration of 10 mM sodium chloride, the dimer dissociation constant was taken from literature.[20] Notably, the dimer dissociation constant K_D can be estimated to be in the order of 250 μM from our plot in Fig. S3 (ESI†). Assuming values for the dimer dissociation constant K_D between 50 μM and 1000 μM

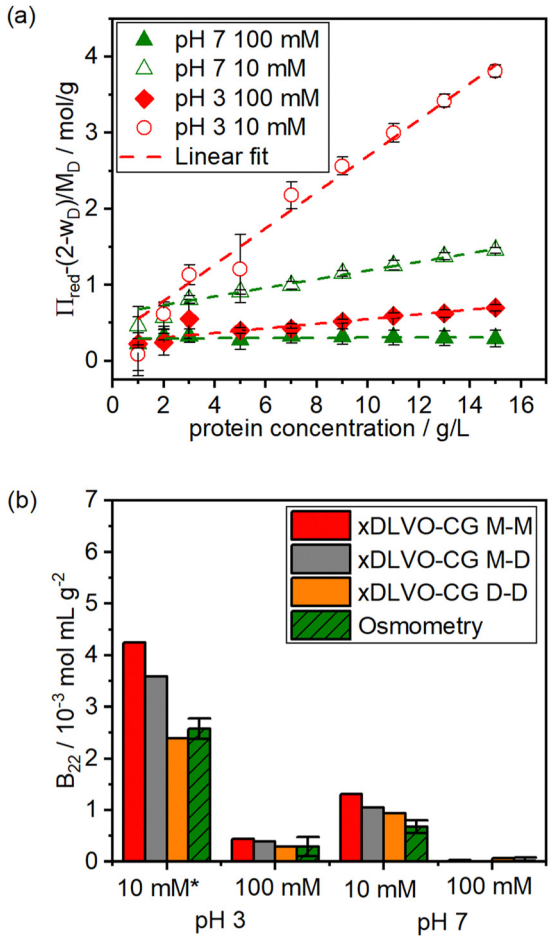

Fig. 7 (a) Experimentally determined molecular weight-corrected osmotic pressure for concentration-dependent molecular weight for BLG in sodium chloride solutions as a function of protein loading concentration. Results are shown for different pH values and salt concentrations. (b) The osmotic second virial coefficient B_{22} for different pH values and sodium chloride concentrations. The coarse-grained xDLVO calculations provide values for monomer–monomer (M–M), monomer–dimer (M–D) and dimer–dimer interactions (D–D). Experimental values are retrieved from a combination of the results from AUC and membrane osmometry (green bars). For a solution pH of 3 and a salt concentration of 10 mM sodium chloride, the dimer dissociation constant for the calculation of the osmotic second virial coefficient was taken from literature.

has only little impact on the evaluation of B_{22} from membrane osmometry data, since the impact of B_{22} on the reduced osmotic pressure is strong in comparison to the dimer dissociation constant K_D in the evaluated protein concentration range.

The influence of non-specific interactions and dimerization due to specific interactions on the reduced osmotic pressure can be seen in Fig. S4-1 (ESI†). Non-aggregating macromolecules with absent or balanced repulsive and attractive interactions yield a straight line with a slope of zero. In the case of pronounced attractive or repulsive intermolecular interactions, a negative or a positive slope is observed, respectively. This is true if the protein concentration is sufficiently low and higher order interactions can be neglected. If, additionally, protein oligomerization occurs, the concentration dependence of the osmotic pressure can no longer be described as a linear function, even at low protein concentrations. For the case of BLG, the decrease of the osmotic pressure due the increase of the dimerization at higher protein loading concentration is superimposed with the influence of binary intermolecular interactions. Since the number of dimers asymptotically approaches a maximum (100%), the number of particles changes less with increasing concentration. Therefore, dimer dissociation directly affects the molecular weight-corrected reduced osmotic pressure at low protein concentrations. This can be observed especially in systems with less pronounced PPIs (see Fig. 7(a) for pH 3, 100 mM; pH 7, 10 mM and 100 mM). Here, dimerization induces an initial decrease in the reduced osmotic pressure. Since the monomer–dimer ratio is less dependent on the protein concentration at higher protein concentrations, an approximately linear dependence of the reduced osmotic pressure is observed, which is largely determined by the extent of non-specific PPIs. To account for the influence of dimerization, the reduced osmotic pressure needs to be corrected in terms of the concentration-dependent molecular weight. Since the osmotic pressure is corrected for specific interactions, a linear fit is obtained as shown in Fig. 7(a). Here, the slope corresponds to B_{22}. The measured B_{22} from membrane osmometry are presented in Fig. 7(b). Moreover, we see that the theoretically calculated values using xDLVO-CG and the experimentally measured osmotic second virial coefficients correlate well. Evidently, B_{22} significantly depends on the charge state of the system, hence higher B_{22} values are obtained at pH 3 than at pH 7. As stated before, the charge screening reduces the extent of the non-specific interactions, which is controlled through the salt concentration. These findings are directly in line with literature.[11,52]

In addition, the measured values for B_{22} from membrane osmometry reveal a strong contribution from dimer–dimer interactions, when comparing with the theoretical predictions. This observation is in line with the fact that the monomer–dimer equilibrium is predominantly shifted towards dimers at protein concentrations above 2.5 g L^{-1}, which has been revealed by our AUC measurements. This is further visualized in Fig. S5 (ESI†), which shows the theoretical weight fraction of BLG monomers and dimers for an equilibrium constant of 39.7 μM. Therefore, considering eqn (15), the slope from molecular weight-corrected osmotic pressure in Fig. 7(a) is strongly influenced by dimer–dimer interactions, which is directly reflected by our results.

We have further supported our argument by theoretical calculations of the osmotic second virial coefficient for various protein concentrations based on eqn (15), which is presented in the left panel of Fig. S4-2 (ESI†). For the calculations, the values for the self-interactions B_{MM}, B_{DD} as well as the cross-term interactions B_{MD} were taken from the xDLVO-CG calculations, which are presented in Fig. 7(a). The results from Fig. S4-2 (ESI†) reveal a strong decrease of the second virial coefficient at small protein loading concentrations (below 2 g L^{-1}) and a further minor decrease of the second virial coefficient with increasing protein loading concentration. These observations

support the argument that our reported experimentally determined second virial coefficients are strongly influenced by dimer–dimer interactions.

Moreover, xDLVO-CG calculations reveal a similar extent of the intermolecular interactions between BLG monomers and dimers as well as their cross-correlation. Notably, this result is in line with our argumentation of the similarity of the individual terms of cross-term interactions and findings in literature from AUC experiments.[50] Furthermore, B_{22} for monomer–monomer interactions is the highest for a solution pH of 3, which is attributed to the strongest repulsion PPIs due to the charged state of the protein and less pronounced dimer formation *via* the dimer binding site, as can be seen in Fig. 2. Similarity of the osmotic second virial coefficients for BLG may be attributed to the fact that interactions between monomer–monomer, monomer–dimer and dimer–dimer are in the same order of magnitude, thus cross-correlations influence the experimental methods only to a minor extent. Moreover, either BLG monomers or BLG dimers are predominantly present, thus a small contribution from higher oligomers does not influence the experiments.

Finally, we have calculated the molecular-weight reduced osmotic pressure for various protein concentrations based on eqn (16), which is presented in the right panel of Fig. S4-2 (ESI†). While minor experimental uncertainties prevent a direct comparison of the theoretical and experimental data, the slope of the theoretical curves are in line with our experimental results from Fig. 7(a). Notably, all protein concentrations in Fig. 7(a) are provided as weight concentration. This is due to the fact that the data must be in accordance with eqn (13) for the evaluation, which requires c_w as protein weight concentration. Moreover, a direct determination of self-interaction terms B_{MM} and B_{DD} and cross-term interactions B_{MD} from the experimental data was not possible as fitting of the data is associated with too many fitting parameters and minor experimental uncertainties in the measured osmotic pressure.

Following our results from Table 1 and Fig. 7, we believe to have provided a comprehensive tool to determine the extent of PPIs for the dynamically interacting system BLG with a concentration-dependent monomer–dimer equilibrium by a combination of AUC and membrane osmometry measurements. We show the determination of the osmotic second virial coefficient based on a molecular weight-corrected reduced osmotic pressure as a function of the protein loading concentration. In this context, our experimental protocol allows the quantification of the effect of self-dissociation, charge–charge interactions and vdW interactions at the same time. Notably, the measured second virial coefficients show positive values, which indicates global repulsive protein–protein interactions.[45]

Relationship between the osmotic second virial coefficient and the dimer dissociation energy

In the final part of this manuscript, we aim towards relating non-specific protein interactions and dimer dissociation from an experimental as well as theoretical point of view. The extent of specific interactions for the BLG system was retrieved from free energy calculations using the US technique. The Gibbs free energy ΔG is directly related to the dimer dissociation constant through the following relationship:[88]

$$\Delta G = RT\ln(K_D) \tag{26}$$

From eqn (26), it is evident that the dissociation energy directly scales with the thermal energy k_BT. The free energy of the BLG monomers is significantly promoted at pH 7 and the BLG binding energy is -8.3 kcal mol^{-1} and -6.9 kcal mol^{-1} at salt concentrations of 10 mM and 100 mM sodium chloride, respectively, as can be seen in Fig. 8(a). These values correlate well with the available experimental data.[89] The binding free energy of the BLG dimer at pH 3 is less favorable, approximately -4.2 kcal mol^{-1} at a salt concentration of 100 mM sodium chloride and shows less pronounced dimerization. It is worth noting that at this buffer condition, the binding of the BLG still has an attractive character, therefore, both forms of BLG are present.

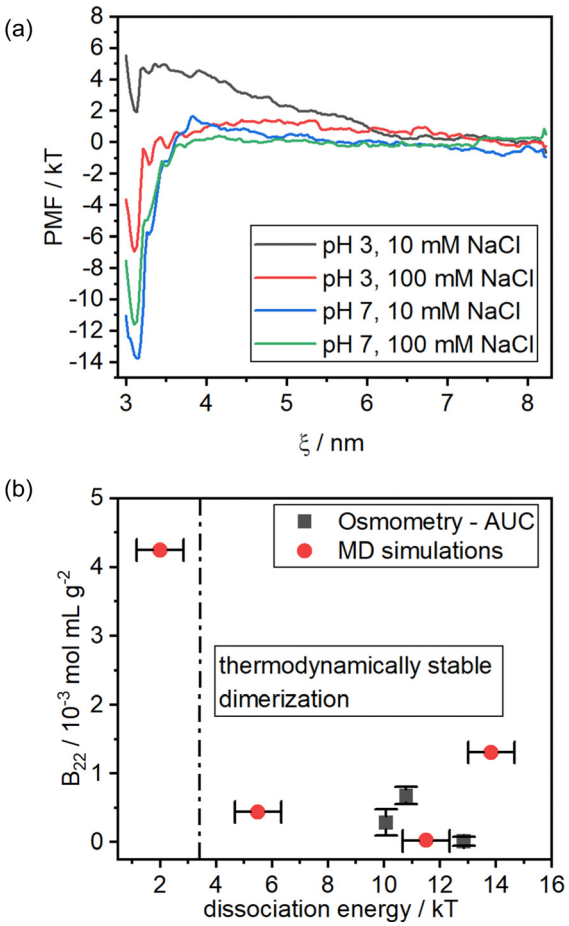

Fig. 8 (a) Free energy of BLG dimerization at different studied solution conditions obtained from umbrella sampling simulations at 300 K and atmospheric pressure. (b) Second virial coefficient from membrane osmometry as a function of the dissociation energy as determined from SV-AUC (red circles). The experimental results are compared with the theoretical results from xDLVO-CG (B_{22}) for monomer–monomer interactions and MD/US simulations for the Gibbs free energy (black circles).

Notably, this is in accordance with results from AUC experiments, as can be seen in Fig. 5. Contrary to that, if the salt concentration is lower (green curve in Fig. 8(a), *i.e.* 10 mM sodium chloride, dimerization of the BLG is suppressed and higher amounts of BLG monomers are present. The binding energy of the BLG dimer in this case is positive (+1.2 kcal mol ^{1}), therefore, the formation of the BLG dimer is thermodynamically unstable. Finally, we summarize our theoretical predictions from xDLVO-CG (B_{22} coefficients) and MD simulations with US free energy calculations (ΔG) in Fig. 8(b). Notably, all umbrella sampling histograms and calculated PMF are provided in Fig. S6 and S7 (ESI†).

For a comparison of theoretical and experimental results, our measured dissociation constants (Table 1) were converted to Gibbs free energy using eqn (26). To establish the relationship between B_{22} and dissociation constant of BLG system, we combined the experimental data for the non-specific interactions from membrane osmometry, which are represented by the second virial coefficient and the measured dimer Gibbs free energy, which is provided in Fig. 8(b). Notably, we did not consider the data point for a solution pH of 3 and a salt concentration of 10 mM sodium chloride for two reasons. First, we could not directly measure the dissociation constants by AUC due to a significant influence of charge effects. Second, this data point is within the thermodynamically unstable region, as shown by our free energy calculations.

Finally, our results depicted in Fig. 8(b) can be interpreted as follows. On the one hand, the osmotic second virial coefficient relates to the dissociation energy and significantly decreases with an increase of dissociation energies (*i.e.* higher binding energy). Conclusively, the osmotic second virial coefficient can be qualitatively used as a predictor for protein dissociation. Notably, a similar relationship for the second osmotic virial coefficient is established in the context of protein solubility. Moreover, as the supersaturation is directly related to the crystallization, the second osmotic virial coefficient serves as a measure for protein crystallization.[24,90 92] In our manuscript, we point towards establishing a relationship to controlled protein oligomerization.

Furthermore, our experimentally determined values for the Gibbs free energy lie within the thermodynamically stable region for the dimerization. However, the theoretically calculated binding free energies quantitatively match our experimental results only at specific experimental conditions, *i.e.* pH of 7 and 100 mM sodium chloride. Discrepancies between other values of binding energy are attributed to the limited accuracy of density fluctuations of salt ions around protein macromolecules during *in silico* free energy calculation. Moreover, while our experimental results are based on a mixture of two BLG variants (A and B), our simulation were conducted for a single variant A. Minor differences are further attributed to a small difference in temperature during experiments, which directly affects the solution density, hence the sedimentation properties through the product of the partial specific volume of the proteins and the solution density (see eqn (4)). Therefore, the final conclusions can only be drawn in a qualitative manner.

Conclusions

In this manuscript, we studied the dynamic monomer–dimer equilibrium of BLG with two variants (A and B) with respect to PPIs based on a unique combination of AUC and membrane osmometry measurements. While the dimer dissociation constant is provided from AUC experiments, the molecular weight-corrected osmotic pressure from membrane osmometry provides the second osmotic virial coefficient for the dynamically interacting system BLG. With this protocol at hand, both specific and non-specific PPIs between BLG species were investigated at a solution pH of 3 and 7 and two salt concentrations in order to mimic technical conditions, namely 10 mM and 100 mM of sodium chloride. While specific interactions were accounted for by the dissociation constant as measured by SV-AUC, we determined the extent of non-specific interactions with the osmotic second virial coefficient by means of membrane osmometry. Data analysis revealed a strong dependence of the dimer dissociation on the charge state of the protein, which is controlled by the solution pH. These findings are in line with literature. Our measured values agree well with predictions from an extended xDLVO-CG approach, which was applied to calculate PPIs between BLG at different solution conditions and charge states from B_{22} coefficients. With this unique combination of the two techniques, we provide an experimental protocol to study specific interactions, *i.e.* dimerization and non-specific interactions at the same time for a dynamically interacting system such as BLG. Finally, we evaluated our experimental approach by analyzing the relationship between the osmotic second virial coefficients, which represents the extent of non-specific intermolecular interactions, and to the BLG dimer dissociation constant.

In order to predict the binding free energies of the BLG oligomerization, umbrella sampling simulations were performed. A thermodynamically stable and unstable region was revealed by the extent of the binding energy. Finally, a comparison of the experimentally measured and theoretically calculated Gibbs free energies was possible in a qualitative manner. As the contribution of the osmotic pressure of the solution is proportional to the number of molecules in solution, this is further directly related to the dimerization constant. Therefore a relationship of the two phenomena was addressed in our manuscript. Our experimental protocol aims towards enabling the determination of the osmotic second virial coefficient, which will serve as a predictor for the BLG protein dissociation. This conclusion points towards establishing a structure–property relationship for controlled prediction of protein oligomerization. Finally, the study of genetically modified BLG variants may serve as a promising model system for further studies including the application of AUC to the determination of the second virial coefficient with a specific focus on the determination of cross-term interactions.

Author contributions

MJU: conceptualization, visualization, investigation, writing – review and editing. CH: investigation, visualization, writing –

review and editing. VL: conceptualization, investigation, visualization, writing and editing. SP: investigation, investigation, visualization, writing and editing. SB: investigation and writing. TRH: conceptualization, writing and editing. JKK: conceptualization, writing and editing, supervision, funding acquisition. WW: supervision, funding acquisition, resources. MK: conceptualization, visualization, supervision, writing – review and editing. JW: conceptualization, investigation, writing – review and editing. AMW: conceptualization, review and editing, supervision, resources. WP: conceptualization, review and editing, funding acquisition, supervision, resources.

Conflicts of interest

There are no conflicts to declare.

Acknowledgements

All authors acknowledge funding through the priority program SPP 1934. SP, MK and WW acknowledge project WE1863/30-2. MJU, JW and WP gratefully acknowledge funding by DFG through project INST 90-1123-1 FUGG. M. K. acknowledges funding by the Ministry of Science, Research and Art of Baden-Württemberg Germany) under Brigitte-Schlieben-Lange-Programm.

References

1 P. Braun and A.-C. Gingras, History of protein-protein interactions: From egg-white to complex networks, *Proteomics*, 2012, **12**, 1478–1498.

2 A. Boire, D. Renard, A. Bouchoux, S. Pezennec, T. Croguennec, V. Lechevalier, C. Le Floch-Fouéré, S. Bouhallab and P. Menut, Soft-Matter Approaches for Controlling Food Protein Interactions and Assembly, *Annu. Rev. Food Sci. Technol.*, 2019, **10**, 521–539.

3 E. Dickinson, Proteins at interfaces and in emulsions Stability, rheology and interactions, *Faraday Trans.*, 1998, **94**, 1657–1669.

4 T. Nicolai, Gelation of food protein-protein mixtures, *Adv. Colloid Interface Sci.*, 2019, **270**, 147–164.

5 J. N. Israelachvili and B. W. Ninham, Intermolecular forces—the long and short of it, *J. Colloid Interface Sci.*, 1977, **58**, 14–25.

6 S. E. Harding and P. Johnson, The concentration-dependence of macromolecular parameters, *Biochem. J.*, 1985, **231**, 543–547.

7 S. K. Chaturvedi, A. Parupudi, K. Juul-Madsen, A. Nguyen, T. Vorup-Jensen, S. Dragulin-Otto, H. Zhao, R. Esfandiary and P. Schuck, Measuring aggregates, self-association, and weak interactions in concentrated therapeutic antibody solutions, *mAbs*, 2020, **12**, 1810488.

8 S. K. Chaturvedi and P. Schuck, A Reappraisal of Sedimentation Nonideality Coefficients for the Analysis of Weak Interactions of Therapeutic Proteins, *AAPS J.*, 2019, **21**, 35.

9 S. K. Chaturvedi, J. Ma, P. H. Brown, H. Zhao and P. Schuck, Measuring macromolecular size distributions and interactions at high concentrations by sedimentation velocity, *Nat. Commun.*, 2018, **9**, 4415.

10 R. T. Wright, D. B. Hayes, W. F. Stafford, P. J. Sherwood and J. J. Correia, Characterization of therapeutic antibodies in the presence of human serum proteins by AU-FDS analytical ultracentrifugation, *Anal. Biochem.*, 2018, **550**, 72–83.

11 M. J. Uttinger, S. E. Wawra, T. Guckeisen, J. Walter, A. Bear, T. Thajudeen, P. J. Sherwood, A. Smith, A. M. Wagemans and W. F. Stafford, *et al.*, A Comprehensive Brownian Dynamics Approach for the Determination of Non-ideality Parameters from Analytical Ultracentrifugation, *Langmuir*, 2019, **35**, 11491–11502.

12 A. Salis, M. Boström, L. Medda, F. Cugia, B. Barse, D. F. Parsons, B. W. Ninham and M. Monduzzi, Measurements and theoretical interpretation of points of zero charge/potential of BSA protein, *Langmuir*, 2011, **27**, 11597–11604.

13 K. Sakurai, M. Oobatake and Y. Goto, Salt-dependent monomer-dimer equilibrium of bovine beta-lactoglobulin at pH 3, *Protein Sci.*, 2001, **10**, 2325–2335.

14 P. Schuck, *et al., Basic principles of analytical ultracentrifugation*, Boca Raton, CRC Press, 2016, vol. 2015.

15 H. Kieserling, P. Giefer, M. J. Uttinger, V. Lautenbach, T. Nguyen, R. Sevenich, C. Lübbert, C. Rauh, W. Peukert and U. Fritsching, *et al.*, Structure and adsorption behavior of high hydrostatic pressure-treated β-lactoglobulin, *J. Colloid Interface Sci.*, 2021, **596**, 173–183.

16 M. Gottschalk, H. Nilsson, H. Roos and B. Halle, Protein self-association in solution: the bovine beta -lactoglobulin dimer and octamer, *Protein Sci.*, 2003, **12**, 2404–2411.

17 M. Muschol and F. Rosenberger, Interactions in undersaturated and supersaturated lysozyme solutions: Static and dynamic light scattering results, *J. Biol. Chem.*, 1995, **103**, 10424–10432.

18 D. J. Winzor, M. Deszczynski, S. E. Harding and P. R. Wills, Nonequivalence of second virial coefficients from sedimentation equilibrium and static light scattering studies of protein solutions, *Biophys. Chem.*, 2007, **128**, 46–55.

19 Z. Zhu, A. Pius Bassey, Y. Cao, Y. Ma, M. Huang and H. Yang, Food protein aggregation and its application, *Food Res. Int.*, 2022, **160**, 111725.

20 J. K. Keppler, A. Heyse, E. Scheidler, M. J. Uttinger, L. Fitzner, U. Jandt, T. R. Heyn, V. Lautenbach, J. I. Loch and J. Lohr, *et al.*, Towards recombinantly produced milk proteins: Physicochemical and emulsifying properties of engineered whey protein beta-lactoglobulin variants, *Food Hydrocolloids*, 2021, **110**, 106132.

21 S. Khan, R. Ipsen, K. Almdal, B. Svensson and P. Harris, Revealing the Dimeric Crystal and Solution Structure of β-Lactoglobulin at pH 4 and Its pH and Salt Dependent Monomer-Dimer Equilibrium, *Biomacromolecules*, 2018, **19**, 2905–2912.

22 T. R. Heyn, V. M. Garamus, H. R. Neumann, M. J. Uttinger, T. Guckeisen, M. Heuer, C. Selhuber-Unkel, W. Peukert and

J. K. Keppler, Influence of the polydispersity of pH 2 and pH 3.5 beta-lactoglobulin amyloid fibril solutions on analytical methods, *Eur. Polym. J.*, 2019, **120**, 109211.
23 D. Asthagiri, B. L. Neal and A. M. Lenhoff, Calculation of short-range interactions between proteins, *Biophys. Chem.*, 1999, **78**, 219–231.
24 S. Ruppert, S. I. Sandler and A. M. Lenhoff, Correlation between the osmotic second virial coefficient and the solubility of proteins, *Biotechnol. Prog.*, 2001, **17**, 182–187.
25 B. L. Neal, D. Asthagiri and A. M. Lenhoff, Molecular Origins of Osmotic Second Virial Coefficients of Proteins, *Biophys. J.*, 1998, **75**, 2469–2477.
26 S. Pusara, P. Yamin, W. Wenzel, M. Krstić and M. Kozlowska, A coarse-grained xDLVO model for colloidal protein-protein interactions, *Phys. Chem. Chem. Phys.*, 2021, **23**, 12780–12794.
27 R. Srivastava, M. Chattopadhyaya and P. Bandyopadhyay, Calculation of salt-dependent free energy of binding of β-lactoglobulin homodimer formation and mechanism of dimer formation using molecular dynamics simulation and three-dimensional reference interaction site model (3D-RISM): diffuse salt ions and non-polar interactions between the monomers favor the dimer formation, *Phys. Chem. Chem. Phys.*, 2020, **22**, 2142–2156.
28 E. J. W. Verwey, J. T. G. Overbeek and K. van Nes, *Theory of the stability of lyophobic colloids: the interaction of sol particles having an electric double layer*, Elsevier Publishing Company, 1948.
29 T. L. Moore, L. Rodriguez-Lorenzo, V. Hirsch, S. Balog, D. Urban, C. Jud, B. Rothen-Rutishauser, M. Lattuada and A. Petri-Fink, Nanoparticle colloidal stability in cell culture media and impact on cellular interactions, *Chem. Soc. Rev.*, 2015, **44**, 6287–6305.
30 M. Herhut, C. Brandenbusch and G. Sadowski, Inclusion of mPRISM potential for polymer-induced protein interactions enables modeling of second osmotic virial coefficients in aqueous polymer-salt solutions, *Biotechnol. J.*, 2016, **11**, 146–154.
31 M. Kastelic, Y. V. Kalyuzhnyi, B. Hribar-Lee, K. A. Dill and V. Vlachy, Protein aggregation in salt solutions, *Proc. Natl. Acad. Sci. U. S. A.*, 2015, **112**, 6766–6770.
32 S. Qin and H.-X. Zhou, Calculation of Second Virial Coefficients of Atomistic Proteins Using Fast Fourier Transform, *J. Phys. Chem. B*, 2019, **123**, 8203–8215.
33 K. Koga, Osmotic second virial coefficient of methane in water, *J. Phys. Chem. B*, 2013, **117**, 12619–12624.
34 A. C. Stark, C. T. Andrews and A. H. Elcock, Toward optimized potential functions for protein-protein interactions in aqueous solutions: osmotic second virial coefficient calculations using the MARTINI coarse-grained force field, *J. Chem. Theory Comput.*, 2013, **9**, 4176–4185.
35 J. Walter and W. Peukert, Dynamic range multiwavelength particle characterization using analytical ultracentrifugation, *Nanoscale*, 2016, **8**, 7484–7495.
36 P. Schuck, Size-Distribution Analysis of Macromolecules by Sedimentation Velocity Ultracentrifugation and Lamm Equation Modeling, *Biophys. J.*, 2000, **78**, 1606–1619.
37 W. F. Stafford and P. J. Sherwood, Analysis of heterologous interacting systems by sedimentation velocity: curve fitting algorithms for estimation of sedimentation coefficients, equilibrium and kinetic constants, *Biophys. Chem.*, 2004, **108**, 231–243.
38 D. A. Yphantis and D. E. Roark, Equilibrium centrifugation of nonideal systems. Donnan effect in self-associating systems, *Biochemistry*, 1971, **10**, 3241–3249.
39 D. E. Roark and D. A. Yphantis, Studies of self-associating systems by equilibrium ultracentrifugation, *Ann. N. Y. Acad. Sci.*, 1969, **164**, 245–277.
40 W. F. Stafford, Analysis of Nonideal, Interacting, and Non-interacting Systems by Sedimentation Velocity Analytical Ultracentrifugation, in *Analytical Ultracentrifugation*, ed. S. Uchiyama, F. Arisaka, W. F. Stafford and T. Laue, Springer Japan, Tokyo, 2016, pp. 463–482.
41 H. Zhao and P. Schuck, Combining biophysical methods for the analysis of protein complex stoichiometry and affinity in SEDPHAT, *Acta Crystallogr., Sect. D: Biol. Crystallogr.*, 2015, **71**, 3–14.
42 W. Albarracín, I. C. Sánchez, R. Grau and J. M. Barat, Salt in food processing; usage and reduction: a review, *Int. J. Food Sci. Technol.*, 2011, **46**, 1329–1336.
43 C. C. Miller, The Stokes-Einstein law for diffusion in solution, *Proc. R. Soc. London, Ser. A*, 1924, **106**, 724–749.
44 G. M. Pavlov, I. Y. Perevyazko, O. V. Okatova and U. S. Schubert, Conformation parameters of linear macromolecules from velocity sedimentation and other hydrodynamic methods, *Methods*, 2011, **54**, 124–135.
45 A. Solovyova, P. Schuck, L. Costenaro and C. Ebel, Non-Ideality by Sedimentation Velocity of Halophilic Malate Dehydrogenase in Complex Solvents, *Biophys. J.*, 2001, **81**, 1868–1880.
46 M. J. Uttinger, D. Jung, N. Dao, H. Canziani, C. Lübbert, N. Vogel, W. Peukert, J. Harting and J. Walter, Probing sedimentation non-ideality of particulate systems using analytical centrifugation, *Soft Matter*, 2021, **17**, 2803–2814.
47 S. Markutsya, S. Subramaniam, R. D. Vigil and R. O. Fox, On Brownian Dynamics Simulation of Nanoparticle Aggregation, *Ind. Eng. Chem. Res.*, 2008, **47**, 3338–3345.
48 E. Antonopoulou, C. F. Rohmann-Shaw, T. C. Sykes, O. J. Cayre, T. N. Hunter and P. K. Jimack, Numerical and experimental analysis of the sedimentation of spherical colloidal suspensions under centrifugal force, *Phys. Fluids*, 2018, **30**, 30702.
49 A. Hamid, J. J. Molina and R. Yamamoto, Sedimentation of non-Brownian spheres at high volume fractions, *Soft Matter*, 2013, **9**, 10056.
50 J. J. Correia, R. T. Wright, P. J. Sherwood and W. F. Stafford, Analysis of nonideality: insights from high concentration simulations of sedimentation velocity data, *Eur. Biophys. J.*, 2020, **49**, 687–700.
51 C. S. Hundschell, S. Bäther, S. Drusch and A. M. Wagemans, Osmometric and viscometric study of levan, β-lactoglobulin and their mixtures, *Food Hydrocolloids*, 2020, **101**, 105580.
52 H. M. Schaink and J. A. M. Smit, Determination of the osmotic second virial coefficient and the dimerization of

β-lactoglobulin in aqueous solutions with added salt at the isoelectric point, *Phys. Chem. Chem. Phys.*, 2000, **2**, 1537–1541.
53 F. Khoury and D. B. Robinson, Interaction Second Virial Coefficients in Binary Systems, *J. Chem. Phys.*, 1971, **55**, 2071–2075.
54 B. Derjaguin and L. Landau, Theory of the stability of strongly charged lyophobic sols and of the adhesion of strongly charged particles in solutions of electrolytes, *Prog. Surf. Sci.*, 1993, **43**, 30–59.
55 E. Hückel, *Zur Theorie der Elektrolyte*, Ergebnisse der Exakten Naturwissenschaften, Springer Berlin Heidelberg, Berlin, Heidelberg, 1924, pp. 199–276.
56 H. C. Hamaker, The London—van der Waals attraction between spherical particles, *Physica*, 1937, **4**, 1058–1072.
57 S. Asakura and F. Oosawa, Interaction between particles suspended in solutions of macromolecules, *J. Polym. Sci.*, 1958, **33**, 183–192.
58 M. Boström, F. W. Tavares, B. W. Ninham and J. M. Prausnitz, Effect of salt identity on the phase diagram for a globular protein in aqueous electrolyte solution, *J. Phys. Chem. B*, 2006, **110**, 24757–24760.
59 L. A. Moreira, M. Boström, B. W. Ninham, E. C. Biscaia and F. W. Tavares, Effect of the ion-protein dispersion interactions on the protein-surface and protein-protein interactions, *J. Braz. Chem. Soc.*, 2007, **18**, 223–230.
60 B. W. Ninham, On progress in forces since the DLVO theory, *Adv. Colloid Interface Sci.*, 1999, **83**, 1–17.
61 M. Boström, D. R. M. Williams and B. W. Ninham, Surface Tension of Electrolytes: Specific Ion Effects Explained by Dispersion Forces, *Langmuir*, 2001, **17**, 4475–4478.
62 M. Boström, D. R. M. Williams and B. W. Ninham, Specific Ion Effects: Why the Properties of Lysozyme in Salt Solutions Follow a Hofmeister Series, *Biophys. J.*, 2003, **85**, 686–694.
63 M. Boström, F. W. Tavares, S. Finet, F. Skouri-Panet, A. Tardieu and B. W. Ninham, Why forces between proteins follow different Hofmeister series for pH above and below pI, *Biophys. Chem.*, 2005, **117**, 217–224.
64 D. F. Parsons, M. Boström, P. Lo Nostro and B. W. Ninham, Hofmeister effects: interplay of hydration, nonelectrostatic potentials, and ion size, *Phys. Chem. Chem. Phys.*, 2011, **13**, 12352–12367.
65 G. Zocher and T. Stehle, Bovine beta lactoglobulin crystallized through ligandation of yttrium cations, 2011.
66 A. Waterhouse, M. Bertoni, S. Bienert, G. Studer, G. Tauriello, R. Gumienny, F. T. Heer, T. A. P. Beer, C. de Rempfer and L. Bordoli, *et al.*, SWISS-MODEL: homology modelling of protein structures and complexes, *Nucleic Acids Res.*, 2018, **46**, W296–W303.
67 H. Li, A. D. Robertson and J. H. Jensen, Very fast empirical prediction and rationalization of protein pKa values, *Proteins*, 2005, **61**, 704–721.
68 T. J. Dolinsky, P. Czodrowski, H. Li, J. E. Nielsen, J. H. Jensen, G. Klebe and N. A. Baker, PDB2PQR: expanding and upgrading automated preparation of biomolecular structures for molecular simulations, *Nucleic Acids Res.*, 2007, **35**, W522–W525.
69 J. M. Crowther, G. B. Jameson, A. J. Hodgkinson and R. C. J. Dobson, Structure, Oligomerisation and Interactions of β-Lactoglobulin, in *Milk Proteins – From Structure to Biological Properties and Health Aspects*, ed. I. Gigli, InTech, 2016.
70 A. Arkhipov, P. L. Freddolino and K. Schulten, Stability and dynamics of virus capsids described by coarse-grained modeling, *Structure*, 2006, **14**, 1767–1777.
71 W. Humphrey, A. Dalke and K. Schulten, VMD: Visual molecular dynamics, *J. Mol. Graph.*, 1996, **14**, 33–38.
72 J. Huang, S. Rauscher, G. Nawrocki, T. Ran, M. Feig, B. L. Groot, H. de; Grubmüller and A. D. MacKerell, CHARMM36m: an improved force field for folded and intrinsically disordered proteins, *Nat. Methods*, 2017, **14**, 71–73.
73 H. J. C. Berendsen, J. P. M. Postma, W. F. van Gunsteren and J. Hermans, Interaction Models for Water in Relation to Protein Hydration, in *Intermolecular Forces*, ed. B. Pullman, The Jerusalem Symposia on Quantum Chemistry and Biochemistry, Springer Netherlands, Dordrecht, 1981, pp. 331–342.
74 B. Hess, C. Kutzner, D. van der Spoel and E. Lindahl, GROMACS 4: Algorithms for Highly Efficient, Load-Balanced, and Scalable Molecular Simulation, *J. Chem. Theory Comput.*, 2008, **4**, 435–447.
75 H. J. C. Berendsen, J. P. M. Postma, W. F. van Gunsteren, A. DiNola and J. R. Haak, Molecular dynamics with coupling to an external bath, *J. Chem. Phys.*, 1984, **81**, 3684–3690.
76 T. Darden, D. York and L. Pedersen, Particle mesh Ewald: An Nlog(N) method for Ewald sums in large systems, *Biochemistry*, 1993, **98**, 10089–10092.
77 S. Nosé, A unified formulation of the constant temperature molecular dynamics methods, *J. Chem. Phys.*, 1984, **81**, 511–519.
78 M. Parrinello and A. Rahman, Polymorphic transitions in single crystals: A new molecular dynamics method, *J. Appl. Phys.*, 1981, **52**, 7182–7190.
79 J. S. Hub, B. L. Groot and D. de van der Spoel, g_wham—A Free Weighted Histogram Analysis Implementation Including Robust Error and Autocorrelation Estimates, *J. Chem. Theory Comput.*, 2010, **6**, 3713–3720.
80 J. K. Keppler, F. D. Sönnichsen, P.-C. Lorenzen and K. Schwarz, Differences in heat stability and ligand binding among β-lactoglobulin genetic variants A, B and C using (1)H NMR and fluorescence quenching, *Biochim. Biophys. Acta*, 2014, **1844**, 1083–1093.
81 H. Zhao, W. Li, W. Chu, M. Bollard, R. Adão and P. Schuck, Quantitative Analysis of Protein Self-Association by Sedimentation Velocity, *Curr. Protoc. Protein Sci.*, 2020, **101**, e109.
82 S. R. Kar, J. S. Kingsbury, M. S. Lewis, T. M. Laue and P. Schuck, Analysis of transport experiments using pseudo-absorbance data, *Anal. Biochem.*, 2000, **285**, 135–142.
83 D. Hayes, T. Laue and J. Philo, *Program Sednterp: sedimentation interpretation program*, Thousand Oaks, CA, 1995.

84 E. Jurrus, D. Engel, K. Star, K. Monson, J. Brandi, L. E. Felberg, D. H. Brookes, L. Wilson, J. Chen and K. Liles, *et al.*, Improvements to the APBS biomolecular solvation software suite, *Protein Sci.*, 2018, **27**, 112–128.

85 C. A. Brautigam, Calculations and Publication-Quality Illustrations for Analytical Ultracentrifugation Data, *Methods Enzymol.*, 2015, **562**, 109–133.

86 W. Mächtle and L. Börger, *Analytical Ultracentrifugation of Polymers and Nanoparticles, 1. Aufl.*, Springer laboratory; Springer Science & Business Media, Springer-Verlag, s.l., 2006.

87 D. Mercadante, L. D. Melton, G. E. Norris, T. S. Loo, M. A. K. Williams, R. C. J. Dobson and G. B. Jameson, Bovine β-lactoglobulin is dimeric under imitative physiological conditions: dissociation equilibrium and rate constants over the pH range of 2.5-7.5, *Biophys. J.*, 2012, **103**, 303–312.

88 L. C. Xue, J. P. Rodrigues, P. L. Kastritis, A. M. Bonvin and A. Vangone, PRODIGY: a web server for predicting the binding affinity of protein-protein complexes, *Bioinformatics*, 2016, **32**, 3676–3678.

89 R. K. Owusu Apenten and D. Galani, Thermodynamic parameters for beta-lactoglobulin dissociation over a broad temperature range at pH 2.6 and 7.0, *Thermochim. Acta*, 2000, **359**, 181–188.

90 C. Haas, J. Drenth and W. W. Wilson, Relation between the Solubility of Proteins in Aqueous Solutions and the Second Virial Coefficient of the Solution, *J. Phys. Chem. B*, 1999, **103**, 2808–2811.

91 J. Valente, R. Payne, M. Manning, W. Wilson and C. Henry, Colloidal Behavior of Proteins: Effects of the Second Virial Coefficient on Solubility, Crystallization and Aggregation of Proteins in Aqueous Solution, *Curr. Pharm. Biotechnol.*, 2005, **6**, 427–436.

92 B. Guo, S. Kao, H. McDonald, A. Asanov, L. L. Combs and W. William Wilson, Correlation of second virial coefficients and solubilities useful in protein crystal growth, *J. Cryst. Growth*, 1999, **196**, 424–433.